Optimizing Interface Conductivity in Electronics

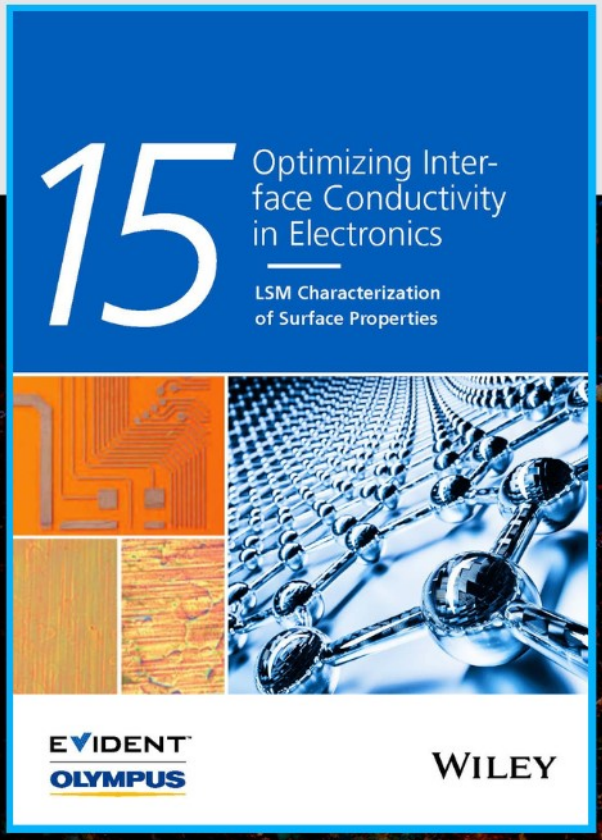

The latest eBook from Advanced Optical Metrology. Download for free.

Surface roughness is a key parameter for judging the performance of a given material's surface quality for its electronic application. A powerful tool to measure surface roughness is 3D laser scanning confocal microscopy (LSM), which will allow you to assess roughness and compare production and finishing methods, and improve these methods based on mathematical models.

Focus on creating high-conductivity electronic devices with minimal power loss using laser scanning microscopy is an effective tool to discern a variety of roughness parameters.

EVIDENT
OLYMPUS

WILEY

ADVANCED FUNCTIONAL MATERIALS
www.afm-journal.de

Spatial Extent of Fluorescence Quenching in Mixed Semiconductor–Metal Nanoparticle Gel Networks

*Marina Rosebrock, Dániel Zámbó, Pascal Rusch, Denis Pluta, Frank Steinbach, Patrick Bessel, Anja Schlosser, Armin Feldhoff, Karen D. J. Hindricks, Peter Behrens, Dirk Dorfs, and Nadja C. Bigall**

In this work, mixing and co-gelation of Au nanoparticles (NPs) and highly luminescent CdSe/CdS core/shell nanorods (NRs) are used as tools to obtain noble metal particle-decorated macroscopic semiconductor gel networks. The hybrid nature of the macrostructures facilitates the control over the optical properties: while the holes are trapped in the CdSe cores, the connected CdSe/CdS NRs support the mobility of excited electrons throughout the porous, hyperbranched gel networks. Due to the presence of Au NPs in the mixed gels, electron trapping in the gold NPs leads to a suppressed radiative recombination, namely, quenches the fluorescence in certain fragments of the multicomponent gel. The extent of fluorescence quenching can be influenced by the quantity of the noble metal domains. The optical properties are monitored as a function of the NR:NP ratio of a model system CdSe/CdS:Au. By this correlation, it demonstrates that the spatial extent of quenching initiated by a single Au NP exceeds the dimensions of one NR, which the Au is connected to (with a length of 45.8 nm ± 4.1 nm) and can reach the number of nine NRs per Au NP, which roughly corresponds to 400 nm of total electron travel distance within the network structure.

1. Introduction

The advanced properties and functionality of nanocrystals and their potential applications inspired numerous studies in the last decade.[1] Nanocrystal gel networks are a unique class of materials consisting of randomly oriented nanoparticles with direct particle contact or ligand-supported linkage. Due to their highly voluminous, porous and lightweight nature, nanocrystal gel networks can be utilized in surface-driven processes like catalysis, energy harvesting or sensing.[2–12] Gel-like network formation from semiconductor NPs can be carried out following different strategies: ligand removal/desorption, ligand exchange, crosslinking, change in pH, addition of cations or electrostatic, and cryoaerogelation.[13–16] As a first and pioneering example from the end of the 20th century, CdS nanocrystals were assembled into a 3D network structures via oxidizing the surface ligands by H_2O_2[17] and CdSe nanocrystals by tetranitromethane (TNM).[18] Further processing of these nanocrystal gel structures opened up new routes toward self-supported cadmium chalcogenide aerogels, where the pore filling liquid medium was exchanged to air using a supercritical drying technique.[18–20] Our group recently employed advanced gelation methods and powerful synthetic control at the nano-, micro-, and macroscale to prepare functional nanocrystal gel structures.[21] For instance, partial removal of the surface ligands leads to interconnected CdSe/CdS dot/rod solvo- and aerogels.[13,14] In such structures, crystal-to-crystal connections between the building blocks facilitate a spatially extended delocalization of excited electrons within the CdS

M. Rosebrock, Dr. D. Zámbó, P. Rusch, D. Pluta, F. Steinbach, P. Bessel, A. Schlosser, Prof. A. Feldhoff, Prof. D. Dorfs, Prof. N. C. Bigall
Institute of Physical Chemistry and Electrochemistry
Leibniz Universität Hannover
30167 Hanover, Germany
E-mail: nadja.bigall@pci.uni-hannover.de

The ORCID identification number(s) for the author(s) of this article can be found under https://doi.org/10.1002/adfm.202101628.

DOI: 10.1002/adfm.202101628

P. Bessel, A. Schlosser, Prof. P. Behrens, Prof. D. Dorfs, Prof. N. C. Bigall
Laboratory for Nano and Quantum Engineering
Leibniz Universität Hannover
30167 Hanover, Germany

K. D. J. Hindricks, Prof. P. Behrens, Prof. D. Dorfs, Prof. N. C. Bigall
Cluster of Excellence PhoenixD (Photonics
Optics and Engineering – Innovation Across Disciplines)
Leibniz Universität Hannover
30167 Hanover, Germany

K. D. J. Hindricks, Prof. P. Behrens
Institute of Inorganic Chemistry
Leibniz Universitat Hannover
30167 Hanover, Germany

Prof. P. Behrens
Cluster of Excellence Hearing4all
30167 Hanover, Germany

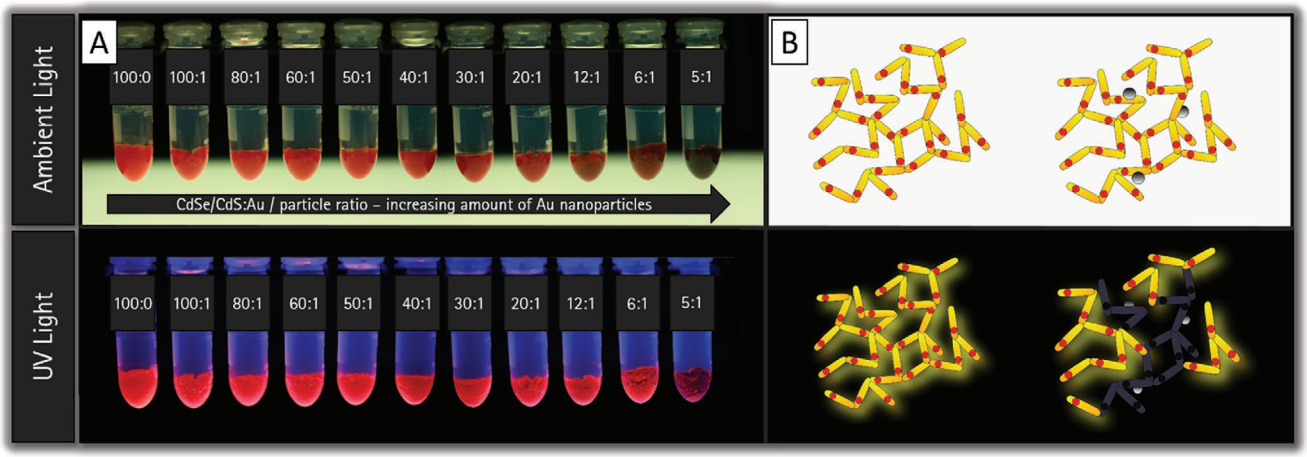

Figure 1. Photographs of mixed nanoparticle hydrogel networks (A) at different CdSe/CdS:Au particle ratios under ambient light (top row) and UV illumination (bottom row). B) Schematic showing the quenching in nanoparticle networks with and without Au NPs. Gray fragments represent the non-fluorescent particles upon quenching.

network, leading to significantly prolonged exciton lifetimes in dried gel networks.[13,14] In contrast, networks formed from silica-coated CdSe/CdS NRs (thus, the semiconductor particles are spatially separated, electronically insulated and therefore decoupled) do not show this optical feature, since the delocalization becomes hindered due to the potential barriers of the silica.[22] Charge carrier dynamics in an interconnected semiconductor NP backbone can be further modified by incorporating noble metal nanoparticles into the network (see schematic **Figure 1**). Due to the position of the Fermi level of noble metals, electrons typically accumulate in the metal domain, opening new non-radiative recombination pathways that manifest themselves in photoluminescence quenching.[23]

In solution ensembles, photoluminescence (PL) quenching was demonstrated for hybrid nanocrystals consisting of Au-decorated CdSe nanorods[24] with different Au domain sizes. Hybrid nanomaterials consisting of co-gelated semiconductor and noble metal nanocrystal (Ag or Au) network further extended the potential applications of such structures in optoelectronic devices as well as in photocatalytic reactions via utilizing the separated electrons and holes in, for example, redox reactions.[25,26]

While synthetic approaches of semiconductor-noble metal mixed gel networks (e.g., CdS-Au/Ag[27,28] and CdTe/Au systems)[29,30] are available, systematic investigation of the spatial extent of the PL quenching as a function of NP ratios in 3D nanocrystal gel networks is still a gap in the literature. To date, the question remained unclear whether one gold particle solely quenches the semiconductor particle it is directly attached to, or also additional neighboring particles located in a certain vicinity of the quencher. By varying the CdSe/CdS:Au particle ratio, the spatial extent of the suppression of the radiative recombination rate can be changed and followed by spectroscopic methods in macroscopic gel structures.

In this paper, the spatial control over the extent of fluorescence quenching is demonstrated in CdSe/CdS-Au mixed nanocrystal gel structures. We show, that in contrast to the colloidal mixtures of the nanocrystal solutions, gelated structures lead to the formation of Au NP-decorated semiconductor NR networks exhibiting partially or almost completely quenched photoluminescence. The optical response of these mixed gel structures can be described as a function of the NR:NP number ratio and the number of quenched NRs per applied Au NP can be estimated. Interestingly, we find that a single quencher has a spatially extended effect: one gold particle efficiently quenches much more than just one semiconductor particle. The photoluminescence of certain gel fragments can be turned off, while others remain optically active, which is a consequence of the spatial distribution of the Au NPs. These findings imply that the photoexcited electrons have a relatively long free paths in the semiconductor backbone. The presented method for the preparation of hyperbranched co-gelated networks can be of great interest in future applications, where an efficient (and tailorable) charge carrier separation is targeted, such as in photoelectrocatalysis, optoelectronics, and spectroelectrochemical sensing.

2. Results and Discussion

Colloidal solution mixtures and gelated mixtures of CdSe/CdS and Au were prepared and compared (see Figure S4, Supporting Information, for the characterization of both building blocks). After mixing and co-gelating the semiconductor nanorods and the Au NPs by means of the partial oxidation of the surface ligands via H_2O_2, a gradual change in the visible color and the emission intensity can be observed as a function of NR:NP ratio (Figure 1). In mixed colloidal solutions (without gelating them), the repulsive interparticle interactions (originating from the presence of 3-mercaptopropionic acid (MPA) on the nanocrystal surfaces)[31] ensure the stability as well as hinder the aggregation of both the nanorods and the nanospheres. Consequently, remarkable changes in the optical properties are not expected to be observed as a function of the NR:NP number ratio except of increased absorption of Au NPs. In contrary, the direct particle–particle contacts evolving during the co-gelation of the NRs and Au NPs have a significant impact on the photoluminescence properties of the gels.

In case of pure CdSe/CdS NRs, gelation leads to ultra-long exciton lifetimes indicating an enhanced electron mobility

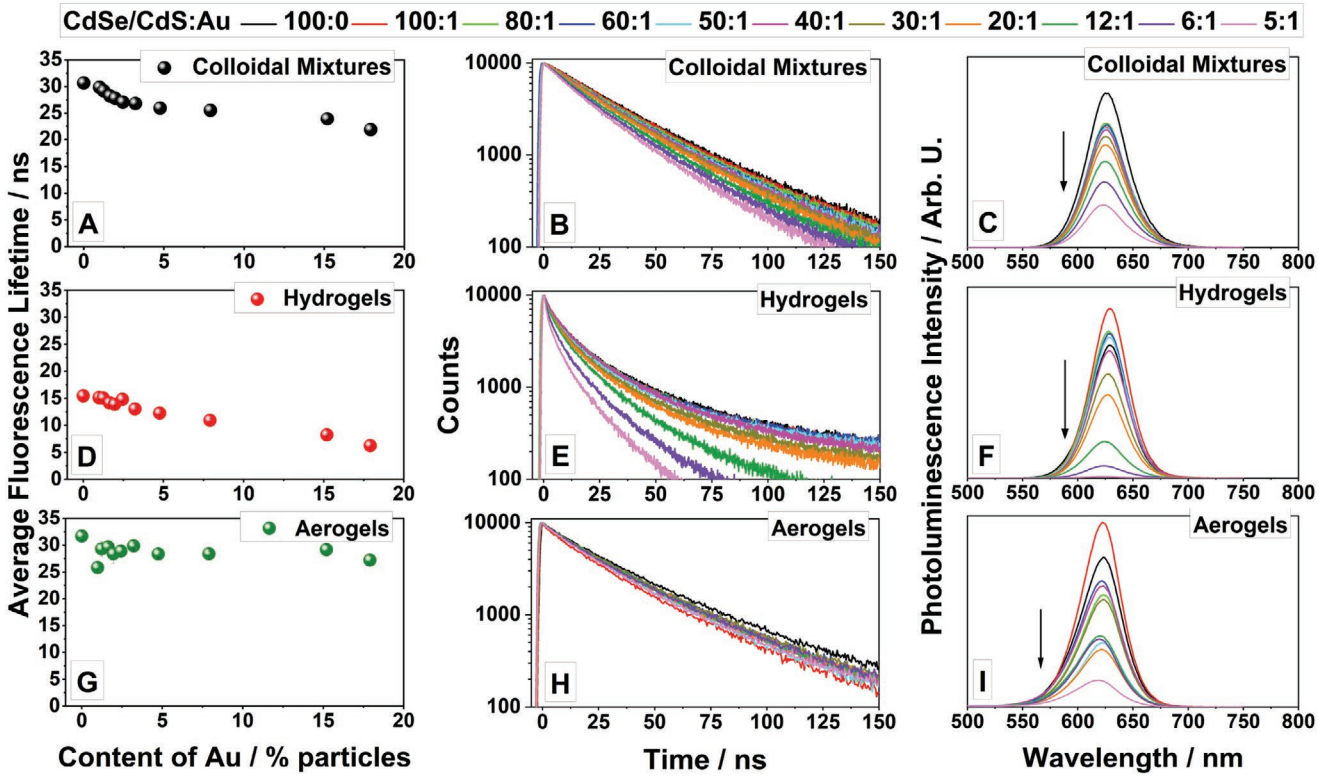

Figure 2. Fluorescence measurements of colloidal mixtures (A–C), hydrogels (D–F), and aerogels (G–I). Average fluorescence lifetimes (left column) of the corresponding decay curves (middle column) and emission spectra (right column).

throughout the gel network.[13,14] Thus, we used this system as a pure NR gel reference in the experiments. To ensure the comparability of the non-gelated mixtures and the co-gelated mixed networks, the same NR and NP concentrations and ratios were used. In the PL measurements, an excitation wavelength of 450 nm was chosen to excite the CdS shell of seeded rods. It is important to point out that this excitation wavelength is off-resonant with the localized surface plasmon resonance of the Au NPs (see Figure S4B, Supporting Information, for details); however, the interband transitions occurring in this wavelength range contribute to the overall absorption in all mixtures. The particles were gelated in aqueous solutions forming hydrogels, which were further processed to prepare acetogels (applying gradual solvent exchange) and aerogels (applying supercritical drying).

Figure 2 shows the average fluorescence lifetimes, fluorescence decay curves and emission spectra of the systems in the form of colloidal mixtures and gels (hydro- and aerogels). Due to the presence of the electrostatically stabilizing surface ligands (MPA for both NRs and NPs), pure CdSe/CdS and Au colloidal solutions possess zeta potentials of −25.8 mV and −27.2 mV, respectively. This provides steric repulsion between the NRs and NPs; however, the reabsorption by Au NPs (see Figure S4B in the SI for Au extinction spectrum) leads to reduced emission intensities at higher particle ratios. Nevertheless, the formation of mixed hydrogels significantly decreases the emission intensities even for low ratios of Au particles to NR. This effect strengthens our hypothesis of delocalized electrons in CdSe/CdS semiconducting gel networks. In the presence of Au NPs within the gel structure, radiative recombination processes of electrons and holes become less favorable and probable; thus, the non-radiative processes become more dominant leading to suppressed PL lifetimes. Au NPs being in direct contact or a suitable distance from the semiconductor backbone are able to quench the PL intensity by accumulating photogenerated electrons. On the other hand, holes are preferentially located in the CdSe cores and later consumed by surface traps and MPA-ligands.[32] The question arises: how many nanorods can be quenched by one Au NP? By loading the network with different numbers of gold NPs, the amount of quenched NRs per Au NP within the gel network can be estimated. However, due to the arbitrary nature of the 3D gel network, this estimation can solely be performed on the basis of the optical properties.

Colloidal solutions and hydrogels show significant differences in terms of photoluminescence lifetime and intensities. This is also valid for the pure semiconductor systems (i.e., without introducing Au NPs), which can be attributed to the oxidative gelation process. The treatment with H_2O_2 leads to the oxidation of the thiolated surface ligands, which manifests in the formation of surface traps facilitating the non-radiative recombination of the photoexcited carriers. However, upon drying, two new effects need to be taken into account: (i) Due to the change in the environment, no solvent molecules are present, and thus, the related non-emissive recombination processes are suppressed; (ii) aerogelation facilitates the enhancement of electron delocalization within the interconnected gel network.[13,14] The presence of Au NPs in the vicinity of the nanorod backbone leads to a fast charge carrier separation: electrons accumulate in the noble metal particles in the *ps* range.[33] Beside the above mentioned processes, this decreases the lifetime in the co-gelated hydrogels to a certain extent governed by

the semiconductor:noble metal particle ratio. As Figure 2A,B demonstrates, the fluorescence lifetime in mixed colloidal solutions does not change significantly upon introducing Au NPs due to the interparticle repulsion between the nanorods and nanoparticles (complete ligand shells protect both type of particles to approach each other in a sufficient extent). In contrast, significant shortening of the photoluminescence lifetime can be observed for the mixed hydrogel networks, where the higher Au content leads to remarkably shorter lifetimes. This effect is the most prominent for CdSe/CdS:Au 6:1 and 5:1 particle ratios (Figure 2E), in which the quenching effect is also the most significant. It is also seen in the emission spectra (Figure 2F) demonstrating an almost completely quenched fluorescence for the ratio of 5:1. (It should be mentioned here, the PL intensity of hydrogels and aerogels is to a certain extent arbitrary and only dependent on the size of the sample in the beam.) This effect cannot be explained solely by the presence of Au NPs and their absorption. The contact between the backbone and the NPs must be sufficient enough to promote the charge carrier separation. Contrary to our expectations, the longer (and quasi constant) PL lifetimes in the aerogel samples indicate that the competition between the electron delocalization and the quenching is not balanced. This implies a prominent effect of the electrical conduction between the backbone and the Au NPs on the optical properties. We observed that the gelation of pure Au NP solutions (with MPA on the surface) does not take place under the same conditions where NRs can be assembled. Therefore, due to the presence of residual ligands, the NPs cannot be in crystal contact with the semiconductor NR surface. While in hydrogels, the contact area is filled with water, so the electrical conductivity (as a consequence of the high dielectric constant of water) can overcome the spatial barrier originating from the gap between the NR and NP. However, aerogelation replaces the solvent by air reducing the permittivity (hence the conductivity) in the contact area significantly.

Furthermore, replacing water with acetone leads to a certain increase in the photoluminescence quantum yield (PLQY or QY), which can be attributed to the lower conductivity of acetone compared to water. To prove this hypothesis experimentally, we tuned the dielectric properties of the solvent in the gap between the semiconductor backbone and the Au NPs. As Figure S9, Supporting Information, shows, the ionic strength within the pore structure of the solvogels affects the extent of charge carrier separation between the CdSe/CdS backbone and Au NPs attached to the network. Additionally, upon changing the solvent from water to non-polar solvents (acetone, hexane and later to air), the PL lifetime and PLQY increase indicating the importance of the dielectric properties of the gap in the quenching process (**Figure 3**A,B).

Figure 3B shows the average fluorescence lifetimes of colloidal mixtures, hydrogels, and selected acetogels as well as aerogels for various Au NP contents. All fluorescence lifetimes are mainly unaffected by the amount of Au NP. This can be attributed to the spatially inhomogeneous quenching in the 3D macrostructure, which strongly affects the QY while the decay dynamics remain unaffected.[34] Since Au^{3+} ions might also be able to quench the fluorescence of the NRs, ruling out of the dissolution of Au NPs is of essential importance. ICP-OES measurements on the sample containing the highest Au NP load clearly prove that the supernatant of the gel samples do not contain Au^{3+} ions (details can be found in Supporting Information). This can be attributed to the chemical stability of Au NPs as well as the thorough washing of the gel samples to eliminate all the impurities from the systems.

Upon connecting individual NRs within the structure, a hyperbranched backbone is formed decorated with Au NPs in a certain extent depending on the NR:NP number ratio

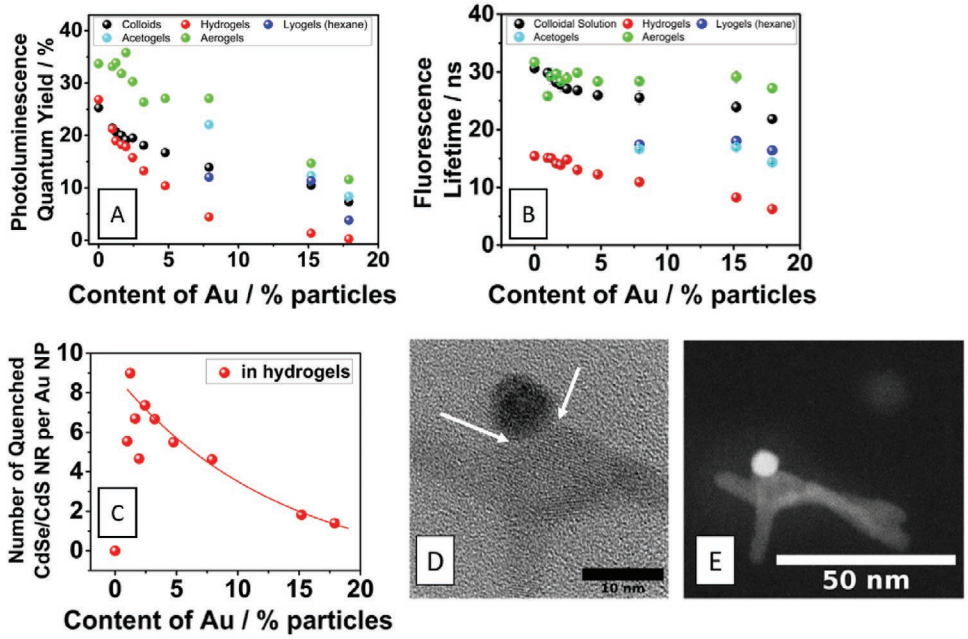

Figure 3. A) Fluorescence lifetimes and B) photoluminescence quantum yields for different Au NP contents. C) Number of quenched NRs as a function of Au NP content estimated from the loss of the QY. D) HRTEM and E) STEM-HAADF images of a selected area showing the attachment of an Au NP to the CdSe/CdS backbone.

(Figure S5, Supporting Information). As a function of the Au content, the mean distances between the quenchers gradually decrease (see Figure S2, Supporting Information). Considering the fact that while the linear distance is highly influenced by the branching of the gel structure (Figure S8, Supporting Information), the travel distances between two quenchers (i.e., the traveled path length of the electron in the backbone) are of higher importance in terms of spatial extent of the quenching. Consequently, we estimate the number of the quenched semiconductor NRs by one Au NP based on the loss of PLQY (Figure 3A) upon increasing Au content. It has to be emphasized that the real path lengths between two quenchers are larger than the radii of the quenched volumes for almost all the investigated NR:NP ratios. Nevertheless, the higher the amount of Au NPs within the network, the more often the quenched volume overlaps. These overlapping quenched volumes (i.e., the quenchers are located closer to each other) can lead to the decrease of the number of quenched NRs per Au NP. Due to the interconnected 3D backbone, the linear distance and the real path lengths between two Au NPs must be differentiated. These important aspects of the systems are demonstrated in Figure S2, Supporting Information, where TEM images as well as schematic 2D slices of the co-gelated networks for two examples (80:1 and 5:1 ratios) are presented.

Interestingly enough, the changes of PLQYs imply that the spatial extent of the quenching—caused by one Au NP—highly exceeds the dimension of a single nanorod. Figure 3C shows that the number of quenched NRs is larger than one for all co-gelated systems. The gradually decreasing number of the quenched NRs is the consequence of the above-mentioned overlapping of the quenched areas. Therefore, the spatial extent of the quenched volume within the network decreases since the quenching of an NR is a binary event and does not depend on the number of quenchers in the vicinity of the NR. Based on the change of the optical properties upon different Au NP loading, up to 9 CdSe/CdS NRs quenched by one gold NP can be estimated. At this maximum value, this roughly equals to 400 nm as total travel distance (using the length of one NR as 45.8 nm ± 4.1 nm).

The estimation is based on PLQY measurements taken from two systems, namely colloidal mixtures and hydrogels (Figure 3A). The details of the calculation can be found in Supporting Information (section Details on Calculation of Quenched Nanorods). For each measurement, the same batch of particles is used, thus, PLQY values are valid for comparison within the same systems using the pure CdSe/CdS NR-based samples (without Au NPs) as references. PLQY values for colloidal mixtures are less affected by an increasing amount of Au NP and show PLQYs of ≈25% for zero Au content to 10% for high Au content with gradual decrease in the whole range of investigated particle ratios (100:1 to 5:1). However, a strong influence of the presence of Au NPs within the gel network structures on the values of PLQY can be observed. With respect to the pure CdSe/CdS hydrogel (value of 26.0%), the Au decorated network structures show a clearly visible trend of gradually decreasing PLQYs with increasing amounts of gold down to 1% of PLQY. In the range of investigated NR:NP ratios, a high excess of rods is present compared to the quencher Au NPs. Moreover, even for the highest Au content (ratio of CdSe/CdS:Au 5:1), the PLQY of the gel network is measurable and the emission is visible by the bare eye (Figure 1A). Based on these findings, it is expected that only a certain portion of the nanorods is quenched for all investigated co-gelated samples. This inhomogeneous quenching manifests itself in a decrease of the PLQY (proportional to the ratio of quenched and non-quenched NRs) as well as in a moderate decrease of the fluorescence lifetime, which typically has a polyexponential decay (as Figure 2E shows). The loss of PLQY in hydrogels of H_2O_2-gelated pure NRs (without additional noble metal NPs) can be attributed to quenching processes mainly caused by surface ligands, surface traps at particle–particle connection areas, and the presence of the solvent. However, these affect the overall network to a similar extent and take also place in the co-gelated networks. Consequently, the sample with NR:NP ratio of 100:0 can be used as a homogeneously quenched reference for comparing the extra quenching effects caused by Au NPs in the mixed samples. Figure 3D,E shows HRTEM and STEM-HAADF images of the CdSe/CdS:Au 5:1 acetogel sample. Here, the distance between the CdSe/CdS NR network and the Au NP was found to be around 1.5 nm ± 0.4 nm. Although the distance indicates an indirect attachment of the Au NP to the network; however, in the presence of a solvent (with relatively high dielectric constant), it can be overcome leading to the quenching of the PL.

Although the determination of the real, physically achievable travel distance is difficult in such systems, the optical properties of the hydrogels (supported by the structural features as well, **Figure 4**) indicate that the quenching effect has a larger spatial extent than the dimensions of a single NR. This leads to an important conclusion: the quenching is not spatially restricted to the vicinity of the NR to which the Au NPs are attached to, but neighboring NRs are also affected (as we schematically visualized in Figure 1B). This also proves the enhanced electron mobility in semiconductor gel structures consisting of interconnected CdSe/CdS nanorods.

Due to the small size of the Au NPs (3.1 nm in diameter, see Figures S4B and S3C, Supporting Information), Au spots are difficult to distinguish by bright-field TEM imaging mode. Additionally, the width of the NRs is also in the same size range; thus, standing nanorods and NPs in the 3D structure give similar contrast in bright field. Detection and visualization of Au components was therefore carried out by scanning transmission electron microscopy coupled with elemental mapping (STEM-EDXS) shown in Figure 4F. Additionally, the composition at the microscale was determined via SEM-EDXS for CdSe/CdS:Au 5:1, 6:1, and 12:1 samples (Figures 4A, 4C, and 4E, respectively). Due to the hyperbranched nature of hydrogel networks, a homogeneous distribution of the noble metal NPs is a crucial requirement to draw the conclusions from macroscopic optical measurements. Figure 4 clearly shows that distribution of Au NPs within the network is homogeneous both on the micro- and on the macroscopic scale. On the one hand, gold is homogeneously distributed in the hyperbranched gel network (Figure 4A,C,E). On the other hand, gold remains in nanoparticle form (as red spots in Figure 4F represent), which also proves that the dissolution of the particles does not occur upon gelation. Co-gelated samples are highly porous and voluminous, and the high specific surface area of the pure semiconductor gel can be retained upon the addition of Au NPs (Figure S7, Supporting Information). We found a BET surface

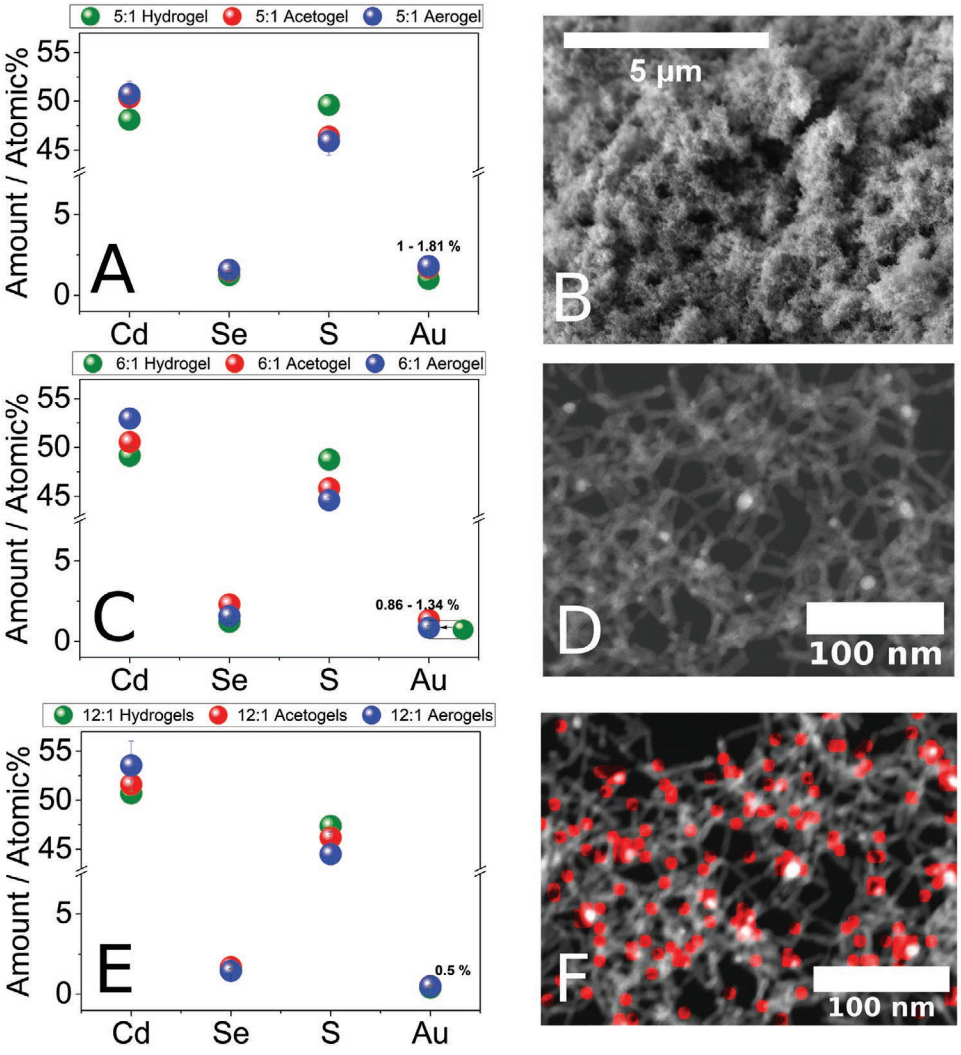

Figure 4. Elemental composition of samples CdSe/CdS:Au A) 5:1, C) 6:1 and E) 12:1 determined by SEM-EDXS. SEM images of B) 5:1 aerogel, D) STEM image and E) elemental mapping of the 5:1 acetogel sample. Red spots correspond to the Au NPs in the co-gelated network.

area of 320 $m^2 \cdot g^{-1} \pm 30$ $m^2 \cdot g^{-1}$ for CdSe/CdS:Au 100:0 sample and 380 $m^2 \cdot g^{-1} \pm 40$ $m^2 \cdot g^{-1}$ for CdSe/CdS:Au 5:1 sample.

Importantly, the micro- and macrostructure of the gels consisting of two components does not differ from those of pure CdSe/CdS gel networks (Figure S5, Supporting Information).

The overall voluminous character of the aerogel prepared from the acetogel of CdSe/CdS:Au 5:1 particle ratio is clearly visible in Figure 4B. It has to be emphasized that the hyperbranched and voluminous nature did not change upon changing the particle ratios: all samples are highly porous regardless of the extent of gold content. Elemental analysis of samples with three different particle ratios is demonstrated in Figures 4A, 4C, and 4E. While sample CdSe/CdS:Au 100:0—with no Au NPs inside—gives no signal for elemental Au, CdSe/CdS:Au 5:1, 6:1, and 12:1 samples contain elemental Au of 1.0 to 1.8 atomic%, 0.9 to 1.3 atomic%, and 0.5 atomic%, respectively. This further proves that Au NPs are strongly attached to the semiconductor backbone and the Au content does not change significantly throughout the preparation of aerogels from aceto- and hydrogels. Even for low amounts of Au NPs in the co-gelated network, the optical properties change drastically (Figure S11, Supporting Information) exhibiting the powerful control over the spatial extent of quenching.

3. Conclusion

An assembly of colloidal mixtures containing semiconductor CdSe/CdS NRs and Au NPs in different particle ratios into gel-like structures has been presented. The prepared hydro-, solvo-, and aeroogels have a hyperbranched semiconductor backbone, in which the NRs are crystal-to-crystal connected facilitating an enhanced mobility of the electrons throughout the network. This backbone has been homogeneously decorated with different number of Au NPs acting as potential quenchers due to their potential to accumulate the excited electrons upon illumination. In contrast to simply mixing the colloidal solutions, fine-tuning the number ratio of the applied NRs and Au NPs within the

gel network has a significant effect on the spatial extent of the quenching processes. Monitoring the optical properties (emission, absorption, quantum yield, and fluorescence lifetime), major differences have been found in the co-gelated structures compared to their colloidally mixed solution counterparts. While the increasing Au content only slightly affects the optical properties in the mixed colloidal solutions at each particle ratios (due to the repulsive interparticle interactions), the gelated networks feature gradual quenching upon increasing gold NP contents. This inhomogeneous quenching shows a certain spatial extent that has been estimated based on the decreasing PLQY proportional to the number of the quenched NRs by one Au NP. The results clearly show that due to the direct interparticle connection within the semiconductor backbone, a single Au NP (with diameter of ≈3.1 nm) is able to quench more than one NR. According to our estimation, up to 9 CdSe/CdS NRs can be quenched by a single Au NP corresponding to ≈400 nm total travel distance of photogenerated electrons. Our findings essentially support the deeper understanding of the co-gelated semiconductor–noble metal architectures, which play an important role in numerous fields of applications such as photo(electro) catalysis and energy harvesting. We demonstrated that mixing and co-gelation offer a simple platform to build up hybrid, multicomponent gel networks, which could be further fine-tuned via the control over the semiconductor–quencher contact and nanoparticle connections in the backbone.

4. Experimental Section

Chemicals: Tri-*n*-octylphosphine oxide (TOPO, 99%), sulfur (S, 99.98%), 1,2,3,4-tetrahydronaphthalene (tetraline, 99%), oleylamine (OAm, 70%), 1-Octadecene (ODE, 90%), 3-mercaptopropionic acid (MPA, 99%) were purchased from Sigma Aldrich. Tri-*n*-octylphosphine (TOP, 97%) was purchased from ABCR. Cadmium oxide (CdO), hydrogen tetrachloroaurate(III) trihydrate ($HAuCl_4 \cdot 3H_2O$, 99.99%), borane *tert*-butylamine complex (TBAB, 97%), and selenium (Se, 99.99%) were purchased from Alfa Aesar. Hexylphosphonic acid (HPA, 99%) and octadecylphosphonic acid (ODPA, 99%) were purchased from PCI Synthesis. All chemicals were used as purchased and without further purification.

Synthesis of CdSe Seeds: CdSe seeds were prepared according to Carbone et al.[35] In a typical synthesis, CdO (0.06 g, 0.47 mmol), ODPA (0.28 g, 0.84 mmol) and TOPO (3.0 g, 7.76 mmol) were mixed in a 25 mL flask and in vacuum heated to 150 °C. After 1 h, the atmosphere was switched to argon and the flask was heated to 300 °C for dissolving the CdO until a clear solution was obtained. TOP (1.8 mL, 4.04 mmol) was added, and the flask was heated to 380 °C. At this temperature, a mixture of TOP (1.8 mL, 4.04 mmol) and Se (0.058 g, 0.73 mmol) was injected into the flask. The reaction was quenched after 4 min by the injection of ODE (4 mL) and the removal of the heating mantle. The flask was cooled down to 90 °C and toluene (5 mL) was added. For purification, the particles were precipitated with methanol (8 mL) and redissolved in hexane (8 mL). This step was repeated twice and the particles were finally stored in hexane (2 mL).

CdSe/CdS Dot-in-Rod Particles: This synthesis was carried out by a seeded-growth method.[35] CdO (0.06 g, 0.47 mmol), HPA (0.08 g, 0.48 mmol), ODPA (0.28 g, 0.84 mmol), and TOPO (9 g, 23.28 mmol) were mixed in a flask and heated up to 150 °C for 1 h in vacuum. After degassing, the atmosphere was switched to argon and the reaction solution was heated to 300 °C until a clear solution was obtained. TOP (1.8 mL, 4.04 mmol) was injected into the flask and the synthesis solution was heated to 350 °C. The prepared spherical CdSe nanoparticles (0.08 µmol) in hexane were dried with air flow and redissolved in a TOP:S mixture (1.8 mL, 4.04 mmol TOP and 0.13 g, 4.05 mmol S) in inert atmosphere. This mixture was quickly injected at 350 °C into the flask by which the temperature decreased to 285 °C. After reaching 350 °C reaction, the temperature was held for 8 min after injection and then air-cooled down to 90 °C and toluene (5 mL) was injected. The purification was carried out by alternating precipitation with methanol (4 mL), centrifugation at 3773 rcf, and redispersion in toluene (4 mL) for at least three times. The final NR solution was stored in toluene (12 mL). The size of the NRs was measured by TEM from organic solution (preferably from chloroform).

Phase Transfer of CdSe/CdS Nanorods: The CdSe/CdS nanorods in organic solution were transferred into aqueous solution by ligand exchange.[31,36] For phase transfer, 12 mL of the nanoparticle solution was precipitated in a mixture of methanol (100 mL), MPA (2.6 mL, 29.84 mmol), and KOH (1.14 g, 20.32 mmol) and shaken for 2 h at room temperature in centrifugation vials. After centrifugation (10 min., 8500 rcf), the precipitate was redispersed in 0.1 M aqueous KOH solution (30 mL). Concentration was determined by atom absorption spectroscopic measurements (AAS).

Synthesis of Au Nanoparticles: Synthesis of the spherical gold nanoparticles was carried out according to Peng et al.[37] $HAuCl_4 \cdot 3H_2O$ (0.1 g, 0.25 mmol), tetraline (10 mL), and OAm (10 mL) were mixed in a flask at room temperature and ambient conditions with stirring for 10 min. TBAB (34.48 mg, 0.40 mmol), OAm (1 mL), and tetraline (1 mL) were sonicated until the TBAB was dissolved. The TBAB solution was quickly injected into the flask and stirred for 2 h at 44 °C. For purification, the nanoparticle solution was divided into parts with a volume of 11 mL, and each sample was precipitated with ethanol (35 mL). After centrifugation (10 min, 8500 rcf), the precipitated nanoparticles were redispersed in toluene (5 mL).

Phase Transfer of Au Nanoparticles: For phase-transfer according to Hiramatsu et al.[38] of the as-prepared spherical nanoparticles, particles in toluene (4.5 mL) were added to a boiling solution of toluene (44 mg, 0.22 mmol nanoparticles in 90 mL toluene). By adding MPA (4.5 mL, 51.64 mmol), the nanoparticles were precipitated as a black solid. After centrifugation (10 min, rcf 8500), the particles were redispersed in 0.1 M KOH (5 mL) followed by precipitation with ethanol (10 mL). This purification step was repeated twice and the particles were finally stored in 0.1 M aqueous KOH solution (3 mL).

Preparation of Hydrogels: Colloidal solutions were mixed according to the calculated particle ratios by keeping the Cd concentration constant (3.6 $mg \cdot mL^{-1}$). After addition of 0.35% H_2O_2 solution (22.2 $\mu L \cdot mg^{-1}$ Cd),[14] samples were well shaken and stored at 80 °C for 90 min in a drying oven. Samples were cooled down and washed several times with ultrapure water to reduce oxidized byproducts and KOH content.

Preparation of Aerogels: After washing with water, solvents in hydrogel samples were exchanged to acetone followed by extra dry acetone. These now called acetogel samples were supercritically dried with liquid CO_2 inside a critical point dryer. Aerogel samples were stored in ambient conditions before measurements took place.

Supporting Information

Supporting Information is available from the Wiley Online Library or from the author.

Acknowledgements

The authors thank the European Research Council (ERC) under the European Union's Horizon 2020 research and innovation program (grant agreement No 714429) for funding. In addition, this work received funding from the German Research Foundation (Deutsche Forschungsgemeinschaft, DFG) under Germany's excellence strategy within the cluster of excellence PhoenixD (EXC 2122, project ID

390833453) and the grant BI 1708/4-1. P.B. is thankful for financial support from the Hannover School for Nanotechnology (HSN). D.D. would like to acknowledge the support by the German Research Foundation (DFG research Grant DO 1580/5-1). Moreover, the authors thank Prof. Denis Gebauer for providing the ICP-OES facility at the Institute of Inorganic Chemistry (LUH) and Kirsten Eiben for the technical assistance. Prof. Peter Behrens would like to thank the Cluster of Excellence EXC 1077/1 "Hearing4all" funded by DFG.

Open access funding enabled and organized by Projekt DEAL.

Conflict of Interest

The authors declare no conflict of interest.

Data Availability Statement

Research data are not shared.

Keywords

aerogels, hydrogels, mixing, multicomponent, nanoparticles, noble metals, semiconductors

Received: February 16, 2021
Revised: May 11, 2021
Published online: June 1, 2021

[1] G. H. Carey, A. L. Abdelhady, Z. Ning, S. M. Thon, O. M. Bakr, E. H. Sargent, *Chem. Rev.* **2015**, *115*, 12732.
[2] J. Fricke, in *Aerogels* (Ed: J. Fricke). Springer, Berlin **1986**, pp. 2–19.
[3] R. D. Gonzalez, T. Lopez, R. Gomez, *Catalysis Today* **1997**, *35*, 293.
[4] N. Hüsing, U. Schubert, *Angew. Chem., Int. Ed.* **1998**, *37*, 22.
[5] A. C. Pierre, G. M. Pajonk, *Chem. Rev.* **2002**, *102*, 4243.
[6] J. Wang, *Analytica Chimica Acta* **2003**, *500*, 247.
[7] X. Luo, A. Morrin, A. Killard, M. Smyth, *Electroanalysis* **2006**, *18*, 319.
[8] Q. Yao, S. L. Brock, *Nanotechnology* **2010**, *21*, 115502.
[9] Z. Yue, F. Lisdat, W. J. Parak, S. G. Hickey, L. Tu, N. Sabir, D. Dorfs, N. C. Bigall, *ACS Appl. Mater. Interfaces* **2013**, *5*, 2800.
[10] L. Korala, J. R. Germain, E. Chen, I. R. Pala, D. Li, S. L. Brock, *Inorg. Chem. Front.* **2017**, *4*, 1451.
[11] D. Wen, A. Eychmüller, *Chem. Commun.* **2017**, *53*, 12608.
[12] A. Schlosser, L. C. Meyer, F. Lübkemann, J. F. Miethe, N. C. Bigall, *Phys. Chem. Chem. Phys.* **2019**, *21*, 9002.
[13] D. Zámbó, A. Schlosser, P. Rusch, F. Lübkemann, J. Koch, H. Pfnür, N. C. Bigall, *Small* **2020**, *16*, 1906934.
[14] S. Sanchez-Paradinas, D. Dorfs, S. Friebe, A. Freytag, A. Wolf, N. C. Bigall, *Adv. Mater.* **2015**, *27*, 6152.
[15] F. Matter, A. L. Luna, M. Niederberger, *Nano Today* **2020**, *30*, 100827.
[16] B. Cai, V. Sayevich, N. Gaponik, A. Eychmüller, *Adv. Mater.* **2018**, *30*, 1707518.
[17] T. Gacoin, L. Malier, J. Boilot, *Chem. Mater.* **1997**, *9*, 1502.
[18] I. U. Arachchige, S. L. Brock, *J. Am. Chem. Soc.* **2007**, *129*, 1840.
[19] J. L. Mohanan, S. L. Brock, *J. Non-Cryst. Solids* **2004**, *350*, 1.
[20] J. L. Mohanan, I. U. Arachchige, S. L. Brock, *Science* **2005**, *307*, 397.
[21] P. Rusch, D. Zámbó, N. C. Bigall, *Acc. Chem. Res.* **2020**, *53*, 2414.
[22] P. Rusch, B. Schremmer, C. Strelow, A. Mews, D. Dorfs, N. C. Bigall, *J. Phys. Chem. Lett.* **2019**, *10*, 7804.
[23] D. Zámbó, A. Schlosser, R. T. Graf, P. Rusch, P. A. Kißling, A. Feldhoff, N. C. Bigall, *under review* **2021**.
[24] T. Mokari, E. Rothenberg, I. Popov, R. Costi, U. Banin, *Science* **2004**, *304*, 1787.
[25] L. Nahar, R. J. A. Esteves, S. Hafiz, U. Oezguer, I. U. Arachchige, *ACS Nano* **2015**, *9*, 9810.
[26] S. P. Bhaskar, M. S. Karthika, B. R. Jagirdar, *ChemistrySelect* **2018**, *3*, 6638.
[27] S. K. Gill, L. J. Hope-Weeks, *Chem. Commun.* **2009**, *29*, 4384.
[28] S. K. Gill, P. Brown, L. J. Hope-Weeks, *J. Sol-Gel Sci. Technol.* **2011**, *57*, 68.
[29] T. Hendel, V. Lesnyak, L. Kühn, A.-K. Herrmann, N. C. Bigall, L. Borchardt, S. Kaskel, N. Gaponik, A. Eychmüller, *Adv. Funct. Mater.* **2013**, *23*, 1903.
[30] S. Sekiguchi, K. Niikura, N. Iyo, Y. Matsuo, A. Eguchi, T. Nakabayashi, N. Ohta, K. Ijiro, *ACS Appl. Mater. Interfaces* **2011**, *3*, 4169.
[31] T. Kodanek, H. M. Banbela, S. Naskar, P. Adel, N. C. Bigall, D. Dorfs, *Nanoscale* **2015**, *7*, 19300.
[32] M. Abdellah, S. Zhang, M. Wang, L. Hammarström, *ACS Energy Lett.* **2017**, *2*, 2576.
[33] D. Mongin, E. Shaviv, P. Maioli, A. Crut, U. Banin, N. Del Fatti, F. Vallée, *ACS Nano* **2012**, *6*, 7034.
[34] J. Maynadié, A. Salant, A. Falqui, M. Respaud, E. Shaviv, U. Banin, K. Soulantica, B. Chaudret, *Angew. Chem., Int. Ed.* **2009**, *48*, 1814.
[35] L. Carbone, C. Nobile, M. De Giorgi, F. D. Sala, G. Morello, P. Pompa, M. Hytch, E. Snoeck, A. Fiore, I. R. Franchini, M. Nadasan, A. F. Silvestre, L. Chiodo, S. Kudera, R. Cingolani, R. Krahne, L. Manna, *Nano Lett.* **2007**, *7*, 2942.
[36] H. G. Bagaria, E. T. Ada, M. Shamsuzzoha, D. E. Nikles, D. T. Johnson, *Langmuir* **2006**, *22*, 7732.
[37] S. Peng, Y. Lee, C. Wang, H. Yin, S. Dai, S. Sun, *Nano Res.* **2008**, *1*, 229.
[38] H. Hiramatsu, F. E. Osterloh, *Chem. Mater.* **2004**, *16*, 2509.